



HAL
open science

Role of defects on high cycle fatigue properties of a cast nickel-based superalloy

Arjun Kalkur Matpadi Raghavendra, Laurent Lacourt, Lionel Marcin, Henry Proudhon, Vincent Maurel

► To cite this version:

Arjun Kalkur Matpadi Raghavendra, Laurent Lacourt, Lionel Marcin, Henry Proudhon, Vincent Maurel. Role of defects on high cycle fatigue properties of a cast nickel-based superalloy. 25ème Congrès Français de Mécanique, Aug 2022, Nantes, France. hal-04345192

HAL Id: hal-04345192

<https://hal.science/hal-04345192>

Submitted on 14 Dec 2023

HAL is a multi-disciplinary open access archive for the deposit and dissemination of scientific research documents, whether they are published or not. The documents may come from teaching and research institutions in France or abroad, or from public or private research centers.

L'archive ouverte pluridisciplinaire **HAL**, est destinée au dépôt et à la diffusion de documents scientifiques de niveau recherche, publiés ou non, émanant des établissements d'enseignement et de recherche français ou étrangers, des laboratoires publics ou privés.



Distributed under a Creative Commons Attribution 4.0 International License

ROLE OF DEFECTS ON HIGH CYCLE FATIGUE PROPERTIES OF A CAST NICKEL-BASED SUPERALLOY

**A.K. Matpadi Raghavendra^{a,b}, L. Lacourt^b, L. Marcin^a, H. Proudhon^b,
V. Maurel^b**

a. Safran Aircraft Engines – Safran Group, Etablissement de Villaroche, France

b. Centres des Matériaux, Mines Paris, PSL university, UMR 7633, France

Résumé :

Les défauts ont un rôle majeur sur la performance en fatigue des pièces de fonderie. La position, la taille, la forme et la densité des pores sont les principaux facteurs de variabilité de la résistance à la fatigue des superalliages base nickel de fonderie. Dans cette étude, des campagnes en fatigue HCF à 750 °C ont été réalisées sur des éprouvettes d'Inconel 100 pour des porosités variables. La microtomographie aux rayons X a été utilisée afin de caractériser en 3D la population de défauts d'un point de vue statistique et morphologique dans le but d'identifier des corrélations avec l'évolution de la durée de vie en fatigue. Les simulations numériques par la méthode des éléments finis ont été réalisées à partir de la reconstruction 3D des défauts réels. Des approches non locales de fatigue, basés sur un critère de fatigue multiaxiale ou sur la mécanique linéaire de la rupture, sont construites à partir du post-traitement des champs mécaniques locaux. La stratégie mise en place permet d'avoir une bonne estimation de l'abatement en fatigue et de la localisation des sites d'amorçage des éprouvettes testées.

Abstract :

The high cycle fatigue (HCF) properties of Inconel 100 have been studied in this work. The samples are tested experimentally and numerically. The main objective of the work is to estimate the effect of clustered defects on HCF properties of the material. Samples with clustered defects are tested at 750 °C under HCF loading and all the samples were found to fail at the zone of clustered defects. For the numerical simulations, image-based finite element (FE) models are developed with the aid of X-ray Computed Tomography (XCT) and a good correlation between experimental and numerical method is established. Various characteristics of defects are analysed via XCT slices and it is seen that there is a large similarity between critical defects of each tested samples, opening the possibilities of a probabilistic fatigue model based on defect statistics. Furthermore, defect's size and its location are the prominent characteristics affecting fatigue life, however, other characteristics cannot be neglected in the case of clustered defects.

Mots clefs : HCF, Clustered defects, Ni-based Superalloys, Image-based FE modelling, XCT

1 Introduction

The material Inconel 100 is a Nickel based superalloy and has its major use in the aviation industry, particularly for turbine discs or blade. However, many defects can be introduced during the casting of the material such as, shrinkages, pores, micro-voids, oxide films etc [1, 2, 3]. These defects are known to degrade the High Cycle Fatigue (HCF) performance of the material. The pores are usually spherical in shape and are formed due to trapped gases or air bubbles while shrinkage driven cavities are caused due to contraction of molten metal during freezing.

The characteristics of these defects play an important role in determining the fatigue life. For example, it is known that surface defect can reduce fatigue life of the material significantly. A surface defect, even if it is 10 times smaller than an internal defect could be more harmful than an internal defect [4, 5]. By the Linear Elastic Fracture Mechanics (LEFM) theory, stress intensity factor (SIF) for an internal defect is given by $K_{I,max} = 0.5\sigma\sqrt{(\pi\sqrt{Area})}$ while for a surface defect, $K_{I,max} = 0.65\sigma\sqrt{(\pi\sqrt{Area})}$ where, Area is the projected area normal to loading direction [5]. Considering that area is same for both the cases, one can estimate that ratio of stress intensity factor for two cracks is $0.65/0.5 = 1.3$ [6, 7]. Therefore, even if the size of surface defect is smaller than sub-surface defect, the crack growth rate quickly overtakes the sub-surface crack growth rate. With all these defect characteristics having prominent impact on material properties, it becomes fairly important to integrate as many as possible effects into numerical model.

Thanks to recent advancements, with the aid of non-destructive methods, it is possible to develop an image based finite element (FE) model that includes real defects using X-ray Computed Tomography (X-ray CT) such that the characteristics are taken into account in the numerical simulations [8]. But, developing and calibrating a model to describe the HCF performance remains a challenging task. Nevertheless, many models have been developed to take into account as many conditions as possible. For long-cracks, the crack propagation threshold can be used to estimate the fatigue limit and has been used by several authors [9]. Moreover, LEFM assumes that fatigue failure is due to one large defect and hence, the model isn't best suited for the case of clustered defects.

A simpler model is the one based on stress concentration factor (SCF). The model states that fatigue limit of a material reduces as much as the SCF from its nominal value in the presence of macrostructural defects or stress concentrating features like notches [10]. The model has been used on other materials and has shown great results [10]. Therefore, this work uses this model to predict the fatigue limit of IN100 specimens.

2 Methods and Procedure

2.1 Material and test setup

Due to the high Ti/Al content (>11%), the two major phases present in IN100 are ordered γ' (Ni_3Al -type) phase embedded in a face-centered cubic (FCC) solid-solution γ -Ni matrix, See Table 1 [11]. Carbides and borides appear as minor phases. Material properties of IN100 depend on a number of interrelated microstructural parameters including the volume fraction of γ' to γ , grain size, elemental distribution, and precipitation of carbides and borides.

Table 1. Composition of Inconel 100

<i>Co</i>	<i>Cr</i>	<i>Al</i>	<i>Ti</i>	<i>Mo</i>	<i>C</i>	<i>B</i>	<i>Zr</i>	<i>Ni</i>
18.4%	12.4%	5.5%	4.5%	3.2%	0.07%	0.02%	0.07%	Balanced

For the current work, four specimens are machined from casted bars. The grains are equiaxed with a size of 1.2 mm and therefore, only factor delimiting fatigue life are defect cavities. The specimens were 40 mm long with a gauge section diameter of 3.7 mm. To test the material under HCF regime, sinusoidal cyclic loads with a load ratio $R=0$ and a frequency of 80 Hz were applied until a maximum of 2×10^6 cycles at a temperature of 750 °C. The specimens were tested using a MTS servo hydraulic machine. Apart from the four samples, samples with no clustered defects were prepared and tested under the same conditions to define the Wöhler curve for a healthy sample. The fatigue life of all the other four test samples are computed with respect to the healthy sample by fatigue reduction factor and is called as *debit* in this article. Debit can be defined as the amplifying factor of stress in the presence of defects, which conversely diminishes the fatigue limit and is given by,

(1)

$$Debit = \frac{\sigma_{alt,healthy} | @ N \text{ cycles}}{\sigma_{alt,sample} | @ N \text{ cycles}}$$

Where $\sigma_{alt,healthy}$ is the fatigue life of healthy samples at N cycles and $\sigma_{alt,sample}$ is the fatigue life of test samples.

2.2 XCT and numerical methods

The test samples were characterized by XCT Nikon XT H 450 set up for a voxel size of $25 \mu\text{m}^3$. The image slices thus obtained were rendered into a volume. The images were treated and segmented using ImageJ software. After the segmentation, the volumes of defects were labelled separately and the surface meshes were extracted. The surface meshes were then inserted into the test sample and were registered in their actual positions, see Figure 1. The volume meshes are generated using ANSA software.

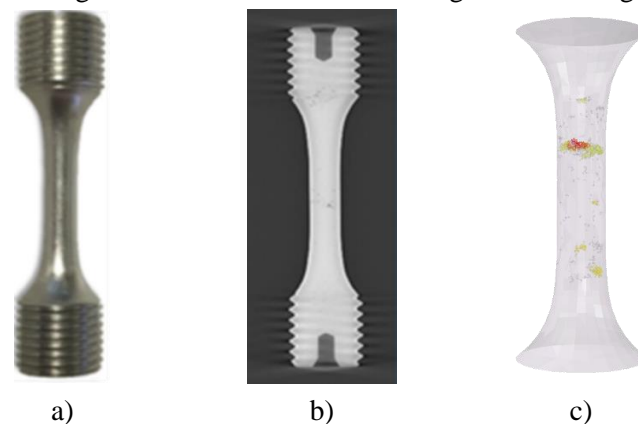


Figure 1. a) Test sample b) X-ray CT scan c) Image based FE model

The developed image based FE models are simulated numerically for one half cycle (tensile part of the cycle at a load ratio $R = 0$) to compute the SCF for ten largest defects of each test sample. In the current work, the failure criterion based on stress concentration is used and therefore it is important to consider the relaxation of stresses and also the evolution of local plasticity in highly stressed regions. So, an isotropic model with kinematic hardening has been adopted to simulate the elasto-viscoplastic behavior of the material.

The hotspots are local maximum stress values (singularities) in the numerical model over which SCFs are computed. To account for stress gradients close to local singularities, volumetric stress homogenization over a sphere with its center on the hotspot is performed. The radius for stress

homogenization is chosen to be 150 μm since it gives the least error in comparison to experimental results.

3 Results and Discussion

3.1 Experimental results

A brief synthesis of the four samples tested are found in Table 2. Along with the four samples, few healthy samples were tested at the same conditions. The Wöhler curves for each sample is shown in Figure 2. To define the wöhler curves, 50% life probability curve from the industrial database is used. The database is created over thousands of tests carried out over the years. Stress amplitudes in Table 2 and Figure 2 are normalized by the fatigue limit of healthy sample due to confidentiality reasons. A scanning electron microscopy analysis revealed the location of crack initiation and the defect that was responsible for the initiation. The debit for each sample is estimated using equation 1.

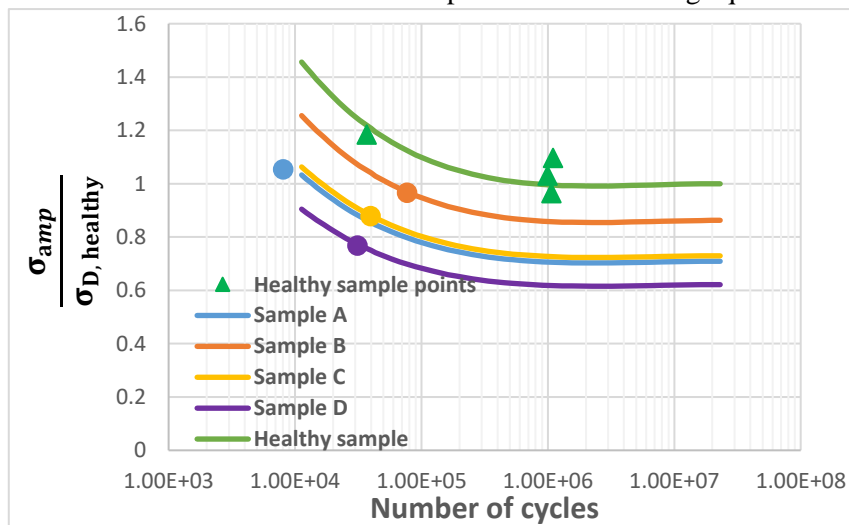


Figure 2. S-N diagram for all the test samples and healthy samples

Table 2. Synthesis of experimental results

No.	Normalized stress amplitude	Number of cycles to failure	Debit	Cause of fracture
A	1.05	8,096	1.4	Shrinkage
B	0.96	77,155	1.15	Shrinkage
C	0.88	39,638	1.35	Shrinkage
D	0.76	31,343	1.6	Shrinkage

In all tested samples, the primary crack initiated from one of the large shrinkage cavities close to surface. In some samples, cracks were found to propagate along the crystallographic plane towards the nearest shrinkage cavity during the early stage of crack propagation as shown in Figure 3. Sample D failed due to a surface defect making it the most critical out of four with a debit of 1.6. The healthy samples did not contain clustered defects but definitely were not defect-free and fractured due to micro shrinkage cavities close to surface. An estimation of porosity along the length of specimen (via XCT slices) reveals that samples failed at the zone of clustered shrinkage as seen in Figure 4.

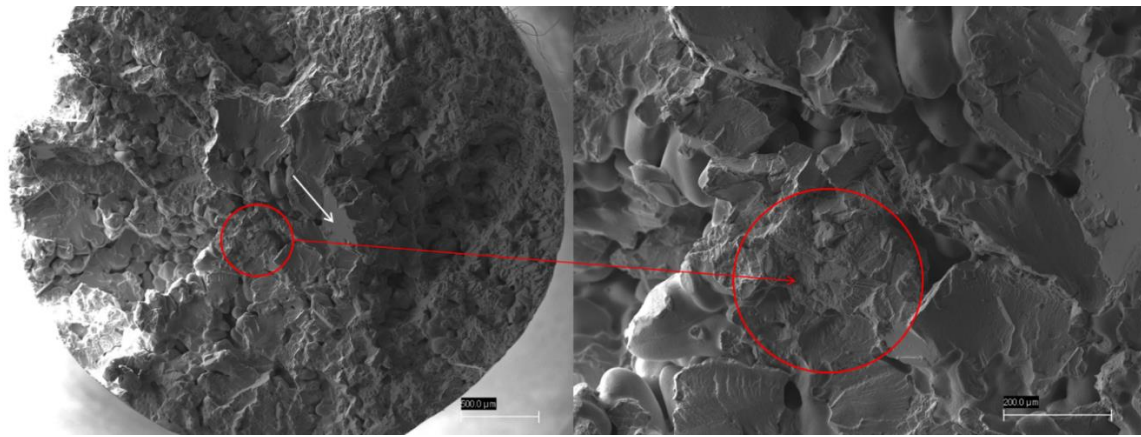


Figure 3. Crack initiation from the shrinkage cavity (image magnified on right) of sample B. The white arrow indicates the propagation of crack along the crystallographic plane.

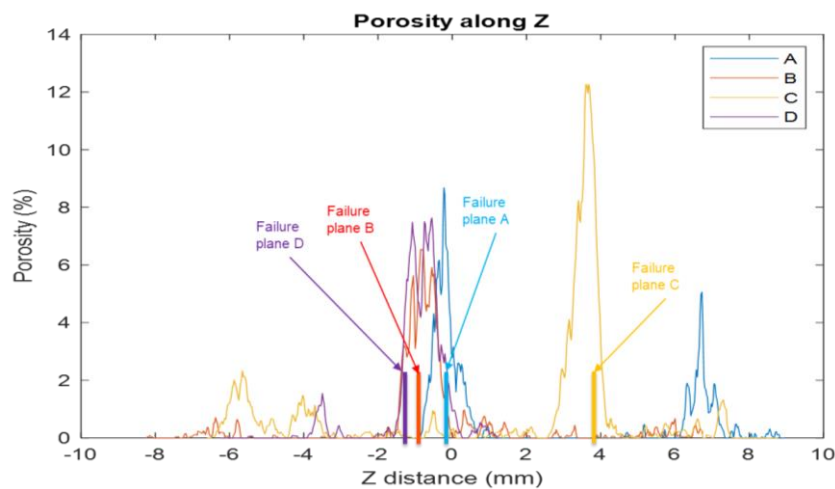


Figure 4. Porosity along the axis of the specimen

Table 3. Synthesis: Characteristics of defects for all the tested samples

Sample A [No. of defects = 92]				Sample B [No. of defects = 175]			
	$\sqrt[2]{Area_{defect}}$	Sphericity	Aspect ratio		$\sqrt[2]{Area_{defect}}$	Sphericity	Aspect ratio
Min	0.056	0.18	1	Min	0.077	0.175	1
Max	1.25	0.71	5.46	Max	1.13	0.67	5.13
Mean	0.22	0.52	1.8	Mean	0.17	0.5	1.93

Sample C [No. of defects = 176]				Sample D [No. of defects = 149]			
	$\sqrt[2]{Area_{defect}}$	Sphericity	Aspect ratio		$\sqrt[2]{Area_{defect}}$	Sphericity	Aspect ratio
Min	0.089	0.125	1.005	Min	0.077	0.18	1.03
Max	1.62	0.7	4.51	Max	0.86	0.65	5.05
Mean	0.19	0.47	2.05	Mean	0.195	0.46	2,1

The XCT image slices are segmented, post-processed and each defect is labelled separately to study their characteristics. A brief synthesis of the defect characteristics for all specimens are found in Table 3. Aspect ratio can be defined as the ratio of major axis to minor axis over a defect projected onto a

plane (here, plane perpendicular to loading) whereas sphericity is a measure of how close a volume is to a sphere. Sphericity can be defined as,

(2)

$$\psi = \frac{(\pi)^{\frac{1}{3}}(6V_p)^{\frac{2}{3}}}{A_p}$$

where, ψ is the sphericity of a defect (the defect is said to be spherical as this value tends to one) V_p , volume of the defect and A_p , surface area of the defect.

It is seen that the number of defects does not have a strong impact on fatigue life. However, if the hierarchy of the defect factors are considered from Table 2, then the size of the defect, sphericity and aspect ratio all seem to follow this order proportionally (the hierarchy as per defect factor is $D > A > C > B$ i.e. defect factor of D is greater than A and so on) except for sample A which needs a further study and analysis on the effects of defect morphology and characteristics of cluster as a whole.

With respect to morphology of defects, defect becomes more and more torturous as the size increases and can be witnessed by the reduction of sphericity, see Figure 5a. From the variation of aspect ratio vs sphericity (see Figure 5b), the defects can be classified into three types: a) Shrinkage cavities b) broken-shrinkage pores and c) Gaseous pores. The large defects with lower sphericity and aspect ratio are the shrinkage cavities while the ones with high sphericity are the gaseous pores and the rest of defects can be termed as broken shrinkage pores which are disconnected from the main shrinkage, hence the large range of aspect ratio.

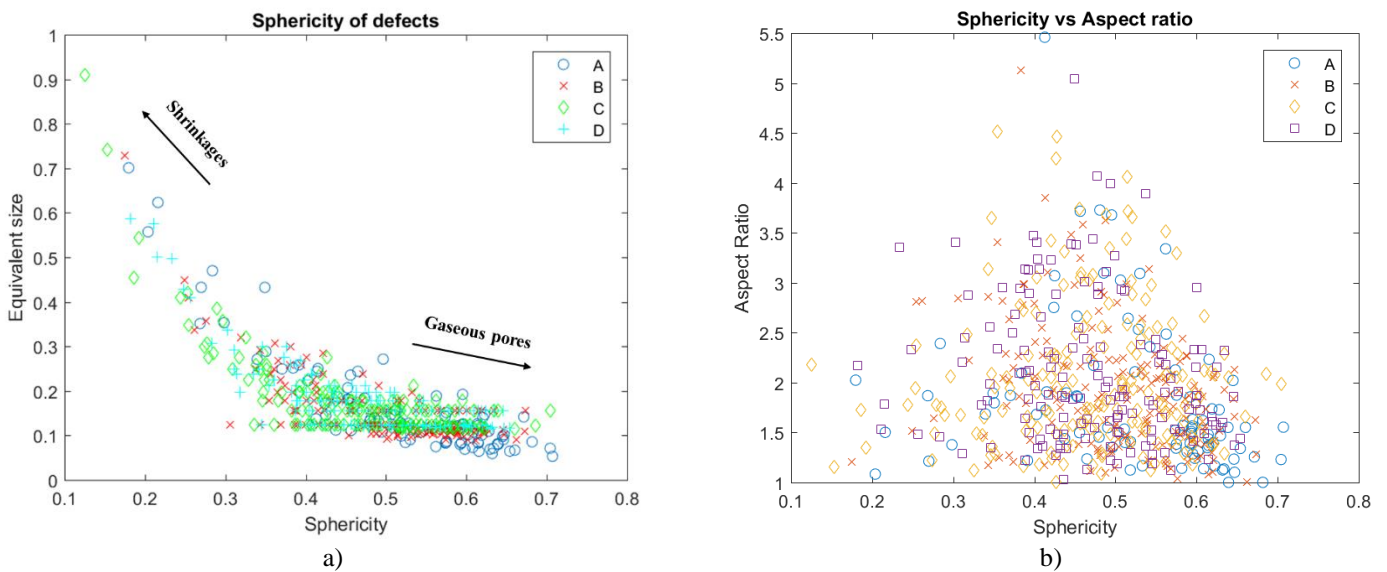


Figure 5.a) Variation of sphericity with respect to defect's size b) Variation of Aspect ratio with respect to sphericity

3.2 Numerical results



Image-based FE models of the samples were simulated for one-half cycle to estimate the SCF and to define the critical pore. A criterion based on SCF is used to determine the fatigue limit of the test samples. According to this criterion, the SCF of the critical defect reduces fatigue limit of tested samples from the materials nominal fatigue limit. The model assumes the material will fail when the averaged stress over a critical volume surrounding the hot spot exceeds the nominal fatigue limit [10]. In this work, the fatigue limit of healthy sample $\sigma_{alt,healthy}$, which is free of large defects and defect clusters would be the nominal fatigue limit. The critical defect of the sample is therefore the one with highest SCF after the Volumetric Stress Homogenization. And so, the criteria is given by

(3)

$$\sigma_D = \frac{\sigma_{D,healthy}}{K_{t,critical}}$$

Where, σ_D is the fatigue limit of the test sample or fatigue life at N number of cycles since the debit factor is assumed to be constant. In this criterion, SCF of critical defect $K_{t,critical}$ is the debit factor that diminishes fatigue limit of the sample. The estimated SCFs (debit factors in this case) are found to be consistent with the experimental debit.

Table 4. Comparison of experimental (exp) and numerical (num) results for test samples: The location of failure and the debit factor. Defect in red contour indicates the critical defect.

Sample A					Sample C				
									
Failure plane Z- position (mm)		Debit			Failure plane Z- position (mm)		Debit		
Exp	Num	Exp	Num	Error (%)	Exp	Num	Exp	Num	Error (%)
± 0	± 0.5	1.4	1.39	-0.3	± 4	± 3.79	1.35	1.52	12

The underlying assumption behind equation 3 is that the crack is supposed to initiate within the volume surrounding the hotspot that exceeds the nominal fatigue limit and therefore, hotspot can be assumed to be the site of crack initiation. From Figure 6, the evaluated crack-initiation site for a specimen and the hotspot are found to be approximately similar validating this statement. In other words, the critical defect responsible for failure is accurately predicted via numerical simulations. Table 3 synthesizes the experimental location of failure along the length (crack-initiation site), numerical hot spot location along the length (predicted critical defect and crack-initiation site) and the debit factors of experimental and numerical methods for two samples. The quadratic average error of the measured debit factors is around 10%.

The characteristics of critical defects show a large similarity as seen in Table 5. From the SEM, optical microscopic and tomographic analysis, it is seen that defect's size and location are the most prominent parameters affecting fatigue life. However, in the case of clustered defects, mechanism of failure is complex and is affected by various parameters which needs a further deep analysis. For example, in sample C, there exists two large defects of size 1.2 and 1.6 mm and both are equidistant from the surface but critical defect is the one of size 1.2 mm. This can be due to morphology of the defect, effect of neighbouring defects or by the influence of other features of defect cluster. Sample D on the other hand, failed from a surface defect and literature evidences prove that surface defect can be very critical to fatigue life [12, 13].

Table 5. Synthesis of characteristics of critical defects

Sample	Defect Size (mm) $\sqrt[2]{Area_{defect}}$	Distance to surface (mm)	Sphericity	Aspect ratio
A	0.72	0.0353	0.2685	1.868
B	1.12	0.025	0.249	1.519
C	1.22	0.07	0.153	1.154
D	0.76	0.106	0.211	1.531

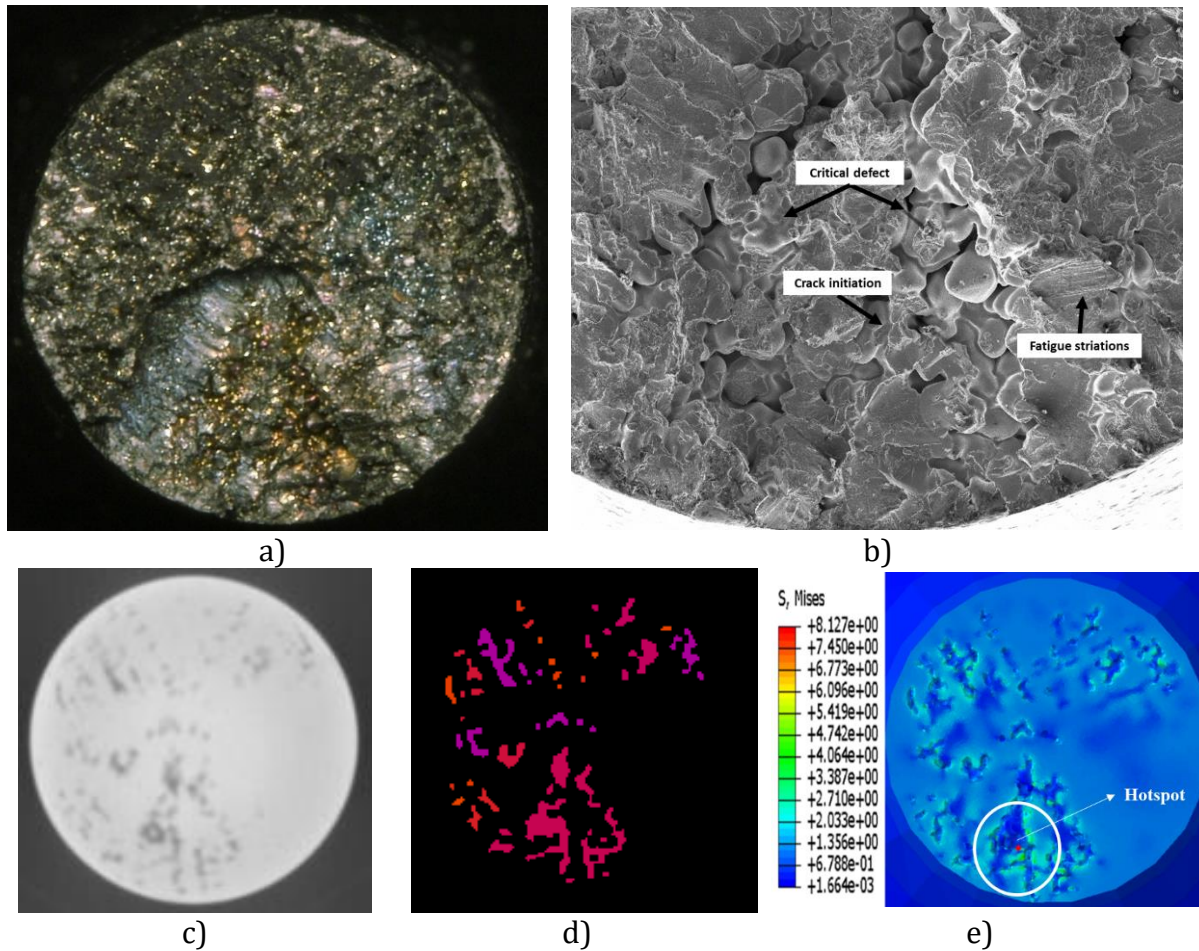


Figure 6. Illustration of the campaign for sample C a) Optical microscopy b) Magnified SEM image of the critical defect c) Tomographic slice of the plane of hot spot d) Segmented image of the same plane (The different colours are the labels assigned for each volume of defect) e) Stress field of the plane containing critical defect and its hot spot

Furthermore, a criterion based on strain energy is also used to predict the number of cycles to failure via numerical simulations until the cycles are stable (i.e. 20 cycles, see Figure 7a). The energy criterion assumes that crack is initiated at the location of maximum energy dissipation on a stable cycle and thereafter remains constant until the failure [14, 15]. The criterion is given by,

(4)

$$dW_p = AN_f^{-k}$$

Where dW_p is the dissipated plastic energy per cycle, N_f is the number of cycles to failure, A and k are the coefficients.

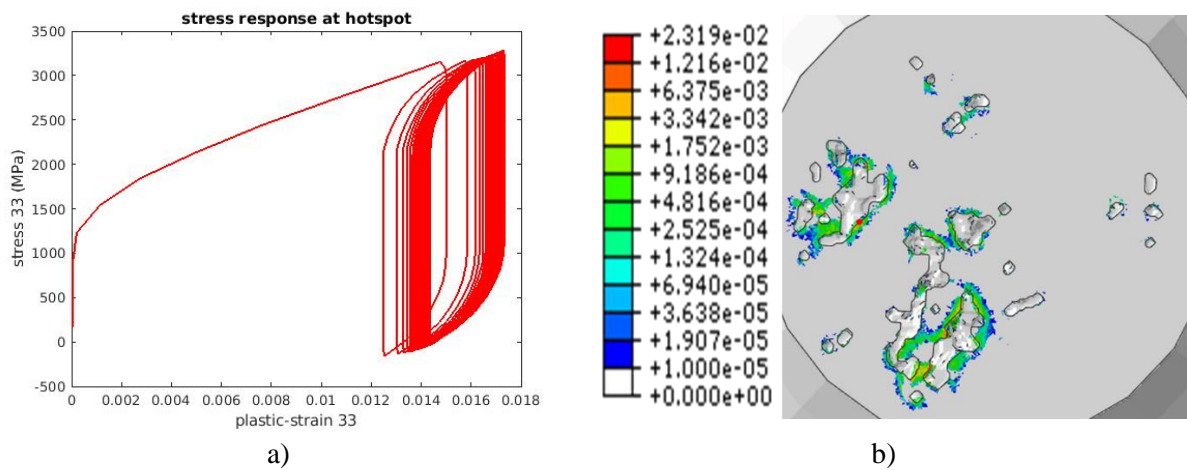


Figure 7. a) evolution of stress vs plastic strain at the hotspot over 20 cycles achieving nearly stable cycle b) Evolution of cumulated plasticity in the local vicinity of defect cluster

The dissipated plastic energy per cycle is measured as,

(5)

$$dW_p = \int_{cycle} \underline{\underline{\sigma}} : \underline{\underline{\varepsilon}}_p dt$$

Where $\underline{\underline{\varepsilon}}_p$ is the plastic strain tensor and $\underline{\underline{\sigma}}$ is the stress tensor. From equation 4, the dissipated plastic energy per cycle is fitted to the number of cycles to failure estimated by experiments to measure the parameters A and k, see Figure 8a. With the known parameters, the number of cycles to failure can be measured. It is also important to note that energy estimations at the local stress and strain peaks needs to be averaged with a characteristic length [16]. This characteristic length is found by varying the length from 100 – 200 μm and evaluating for the least error with respect to fitting of the model: a length (radius) of 150 μm was found to produce best results.

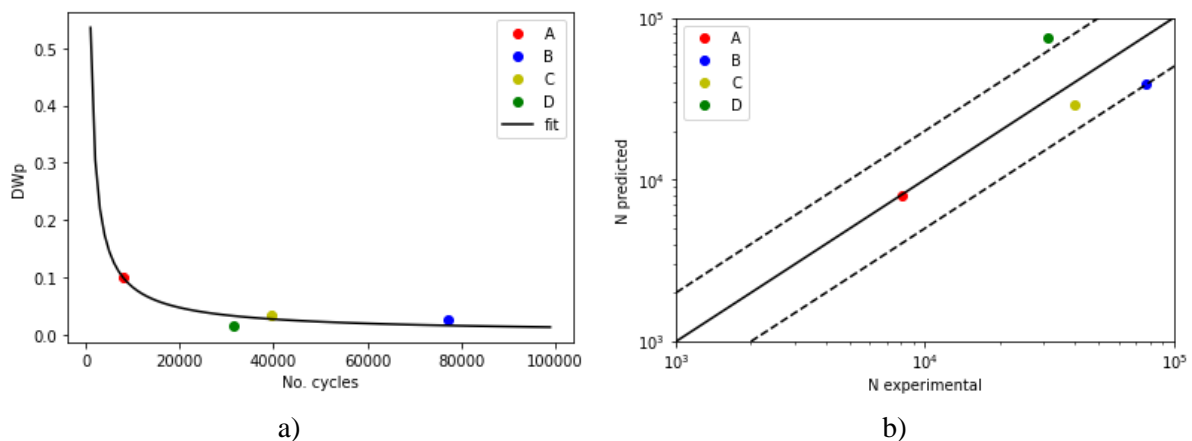


Figure 8.a) Fitting the energy criterion over tested samples b) Predictions of fatigue lives from the fitted criterion

The criterion shows a good fit for all sample, the error is however pretty large for sample D (factor of 2*number of cycles to failure), see Figure 8b. Sample D failed from a surface defect and therefore, the mechanism of failure can be completely different. It should be noted that plasticity evolves over the local vicinity of defects (as seen in Figure 7b) and that model assumes the crack to be initiated from the location of maximum dissipated plastic energy per cycle. This energy dissipated per cycle is assumed to remain constant until failure maintaining an equilibrium with the opening and propagation of crack

where the dissipated energy is spent in propagating the crack while the elastic energy on opening of the crack [16]. Hence, the model is usually efficient and can be used to estimate the integrity of a structure.

4 Conclusion

Ni-based polycrystalline superalloy IN100 containing clustered defects has been studied in this work. After careful analysis of experimental methods, defect characteristics and numerical simulations, following conclusions can be drawn:

1. Experimental and tomographic analysis confirm that all samples failed in the zone of clustered shrinkages.
2. As seen in literature evidences, defect size and location are still the prominent features affecting fatigue life. However, in the case of clustered defect, other characteristics and parameters of cluster on a whole are not negligible and requires further analysis.
3. Due to large similarity among the characteristics of critical defects, the defect population can be funneled down to predict few possible critical defects. This opens up the possibility to develop a fatigue model on the basis of defect characteristics and statistical analysis which relies upon the strategies to generate synthetic microstructures [17].
4. Via a simple model based on SCF, the debit of fatigue limit can be well predicted. A very good correlation between experimental and numerical method has been found in terms of debit, critical defect and crack-initiation site.
5. Criteria based on energy can approximately predict the fatigue life of the material. However, certain specific cases (like surface defect) requires either a better calibrated model or a modification of the existing ones.

References

- [1] F. Nový, P. Kopas, O. Bokůvka, M. Jambor and L. Trško, “Influence of microscopic casting defects on fatigue endurance of ductile cast iron,” *MATEC Web of Conferences*, vol. 157, p. 05019, 2018.
- [2] B. Rutttert, C. Meid, L. M. Roncery, I. Lopez-Galilea, M. Bartsch and W. Theisen, “Effect of porosity and eutectics on the high-temperature low-cycle fatigue performance of a nickel-base single-crystal superalloy,” *Scripta Materialia*, pp. vol. 155, p. 139-243, 2018.
- [3] Y. Nadot, “Fatigue from defect: Influence of size, type, position, morphology and loading,” *International Journal of Fatigue*, vol. 154, 2022.
- [4] A. Rotella, Y. Nadot, M. Piellard, R. Augustin and M. Fleuriot, “Fatigue limit of a cast Al-Si-Mg alloy (A357-T6) with natural casting shrinkages using ASTM standard X-ray inspection,” *International Journal of Fatigue*, vol. 114, p. 177-188, 2018.
- [5] Y. Murakami, “Metal Fatigue: Effects of Small Defects and Nonmetallic Inclusions,” *Elsevier*, 2002.
- [6] Y. Murakami and M. Endo, “Effects of defects, inclusions and inhomogeneities on fatigue strength,” *International Journal of Fatigue*, pp. vol. 16, no 3, p. 163-182, 1994.
- [7] Y. Murakami and S. Nemat-Nasser, “Growth and stability of interacting surface flaws of arbitrary shape,” *Engineering Fracture Mechanics*, pp. vol. 17, no 3, p. 193-210, 1983.
- [8] Y. Hangai, O. Kuwazuru, T. Yano, T. Utsunomiya, Y. Murata, S. Kitahara, S. Bidhar and N. Yoshikawa, “Clustered Shrinkage Pores in Ill-Conditioned Aluminum Alloy Die Castings,” *Materials Transactions*, vol. 51, no. 9, pp. 1574-1580, 2010.

- [9] J.-Y. Buffiere, S. Savelli, P. Jouneau, E. Maire and R. Fougères, “Experimental study of porosity and its relation to fatigue mechanisms of model Al–Si7–Mg0.3 cast Al alloys,” *Materials Science and Engineering: A*, pp. vol. 316, no 1, p. 115-126, 2001.
- [10] D. Taylor, “Geometrical effects in fatigue: A unifying theoretical model,” *International journal of fatigue*, pp. 413-420, 1999.
- [11] T. M. Pollock and S. Tin, “Nickel-Based Superalloys for Advanced Turbine Engines: Chemistry, Microstructure and Properties,” *Journal of Propulsion and Power*, 2006.
- [12] I. Koutiri, E. Pessard, P. Peyre, O. Amlou and T. D. Terris, “Influence of SLM process parameters on the surface finish, porosity rate and fatigue behavior of as-built Inconel 625 parts,” *Journal of Materials Processing Technology*, pp. vol. 255, p. 536-546, 2018.
- [13] A. Yadollahi, N. Shamsaei, S. M. Thompson, A. Elwany and L. Bian, “Effects of building orientation and heat treatment on fatigue behavior of selective laser melted 17-4 PH stainless steel,” *International Journal of Fatigue*, pp. vol. 94, p. 218-235, 2017.
- [14] E. Charkaluk, A. Bignonnet, A. Constantinescu and K. Dang Van, “Fatigue design of structures under thermomechanical loadings,” *Fatigue and fracture of engineering materials and structures*, 2002.
- [15] S. Dezecot, V. Maurel, J.-Y. Buffiere, F. Szymtka and A. Koster, “3D characterization and modeling of low cycle fatigue damage mechanisms at high temperature in a cast aluminum alloy,” *Acta Materialia*, vol. 123, pp. 24-34, 2017.
- [16] V. Maurel, A. Koster, L. Remy, M. Rambaudon, D. Missoum-Benziane, V. Fontanet, F. Salgado-Goncalves, A. Heudt, H. Wang and M. Trabelsi, “Fatigue crack growth under large scale yielding condition: The need of a characteristic length scale,” *International Journal of Fatigue*, vol. 102, pp. 184-201, 2017.
- [17] D. E. Khoukhi, N. Saintier, F. Morel, D. Bellett, P. Osmond and V.-D. Le, “Spatial point pattern methodology for the study of pores 3D patterning in two casting aluminium alloys,” *Material characterization*, vol. 177, 2021.